



Reconstruction of Aeolian Activity Variability in the Central Tibetan Plateau From Grain-Size Distributions: End-Member Modeling and Source Attribution of Sediments From Lake Selin Co

Chunhui Zhang¹, Wanyi Zhang^{1*}, Yan Liu², Jinjiao Yao¹, Renchao Wan¹, Huwei Li¹, Xinyu Hou¹ and Chengjun Zhang¹

¹College of Earth Sciences & Key Laboratory of Mineral Resources in Western China (Gansu Province), Lanzhou University, Lanzhou, China, ²Key Laboratory of Oil and Gas Resources Research, Northwest Institute of Eco-Environment and Resources, Chinese Academy of Sciences, Lanzhou, China

OPEN ACCESS

Edited by:

Yongli Wang,
Institute of Geology and Geophysics
(CAS), China

Reviewed by:

Xianyong Cao,
Institute of Tibetan Plateau Research
(CAS), China
Wenxia Han,
Linyi University, China

*Correspondence:

Wanyi Zhang
zhangwanyi@lzu.edu.cn

Specialty section:

This article was submitted to
Quaternary Science, Geomorphology
and Paleoenvironment,
a section of the journal
Frontiers in Earth Science

Received: 29 January 2022

Accepted: 09 March 2022

Published: 31 March 2022

Citation:

Zhang C, Zhang W, Liu Y, Yao J,
Wan R, Li H, Hou X and Zhang C
(2022) Reconstruction of Aeolian
Activity Variability in the Central Tibetan
Plateau From Grain-Size Distributions:
End-Member Modeling and Source
Attribution of Sediments From Lake
Selin Co.
Front. Earth Sci. 10:865174.
doi: 10.3389/feart.2022.865174

The grain size analysis and end-member modeling of clastic fractions in the Selin Co basin sedimentary sequence have been revealing variations of aeolian activity in the central Tibetan Plateau since 3,900 cal yr BP. The grain-size distributions measured in this study were classified into three statistical end-members that may be connected to clastic material inputs from a variety of sources and transport processes. Among these, the EM3 fraction (modal grain size of ~138 μm) was suggested to indicate the aeolian activity history in the central Tibetan Plateau. The results indicate that the aeolian activity in this region occurred under dry and cold conditions since 3,900 cal yr BP, with three strong aeolian activity intervals at 3,200–2,900 cal yr BP, 2,400–1,400 cal yr BP, and after 130 cal yr BP. Comparison with other records showed that solar insolation, weakening Indian summer monsoon, and the strengthening westerlies have a direct relationship with the aeolian activity in the central Tibetan Plateau. We therefore suggest that the atmospheric circulation patterns and effective humidity may have a strong impact on the water balance and weathering intensity in the arid and semiarid areas, hence affecting dust emissions. Also, the coarse detrital end-member fraction of lake sediments is suggested as a potential aeolian activity proxy.

Keywords: central Tibetan Plateau, Lake Selin Co, end-member analysis, aeolian activity, Indian summer monsoon, the westerlies

1 INTRODUCTION

Aeolian activity has garnered considerable attention from the government and academics as one of the most serious ecological and environmental challenges in Western China. It has a negative impact on human health, contributes to desertification, and has other environmental implications (Okin et al., 2001; Esmaeil et al., 2014). Dust released from aeolian activity plays an active role in modulating global climatic change, and the resulting change, in turn, influences the dust emission (Maher et al., 2010; Wang et al., 2013). Therefore, investigating dust history helps elucidate the

releasing processes and shed light on the mechanisms behind the relationship between dust release and climatic change over time. It contributes to our growing understanding of the ocean–atmosphere–land interactions that govern the climate system. However, the dust storm events inferred from meteorological data and historical archives are insufficient to reconstruct the history of aeolian activity over past periods in the arid and semiarid regions of China, especially paleoenvironmental reconstruction based on environmental proxies is an indispensable method in the areas without history records (Qiang et al., 2007). Additional records from the local region are essential for improving our understanding of regional climate systems.

Lakes in arid regions are natural dust traps resulting in the deposition of continuous sediment that can provide a high-quality sedimentary record for paleoenvironmental changes, especially long-term changes associated with aeolian dust deposition (An et al., 2011; Chen et al., 2013). The nature of dust grain size in lake sediments in the Central Asian arid zone can reflect Asian monsoon system change and wind intensity (Qiang et al., 2007). Therefore, aeolian grain-size distributions (GSDs) from the lake sediments are the most commonly applied proxy in reconstructing past aeolian activity in the Tibetan Plateau region (Chen et al., 2013; Qiang et al., 2014; Wu et al., 2020). Owing to the complexity of the sources of lake sediments, it is important to understand how to distinguish the aeolian fractions and their proportions in lake sediments (Zhang et al., 2021). Several relevant investigations have determined the contribution of aeolian sediments by comparing the grain-size distributions of lake sediments and regional aeolian sediments (Qiang et al., 2007; Qiang et al., 2014). Moreover, several researchers have used mathematical methods to analyze grain size data and build models to identify the sources of various sediments; these models, so-called “end-member models,” have been developed by Paterson and Heslop in 2015. For example, Dietze et al. (2012) applied the end-member modeling analysis (EMMA) on Lake Donggi Cona and identified the following five end-members: EM1 (8.4 ϕ , 3.5 μm) represents suspended sediment from fluvial and alluvial processes, EM2 (6 ϕ , 15.7 μm) represents local dust, EM3 (4.4 ϕ , 47 μm) represents sandy well-sorted, probably dune sediment, EM4 (3 ϕ , 125 μm) represents remote dust, and EM5 (1.7 ϕ , 310 μm) which is poorly sorted, has actually three prominent modes, typical of fluvial and onshore deposition. The end-member model analysis has been successfully applied to determine the aeolian fractions in lake sediments (Chen et al., 2013; Wu et al., 2020; Zhang et al., 2021).

The Tibetan Plateau, which is influenced by the Asian monsoon and the mid-latitude westerlies, is one of Central Asia’s dust-producing regions (Dong et al., 2020). Lake Selin Co, located in the central Tibetan Plateau, is relatively unaffected by human activities. Therefore, it is one of the ideal lakes for studying aeolian activity. Meanwhile, due to its scarce precipitation and a sufficiently large lake surface, the coarse-grained fraction in the sediment at the center of the lake is less influenced by fluvial input (Deckker et al., 1991), which maybe come from air sources. Moreover, previous research has rebuilt the overall framework of monsoonal and paleoenvironmental

changes in the Selin Co region using grain size characteristics, geochemical studies, and isotopic studies (Gu et al., 1993; Morinaga et al., 1993; Kashiwaya et al., 1995; Gyawali et al., 2019). Recent studies (Shi et al., 2017; Hou et al., 2021) used optically stimulated luminescence to date beach ridges in Lake Selin Co to monitor lake-level fluctuation. All previous studies provided basic archives between climate and aeolian activity.

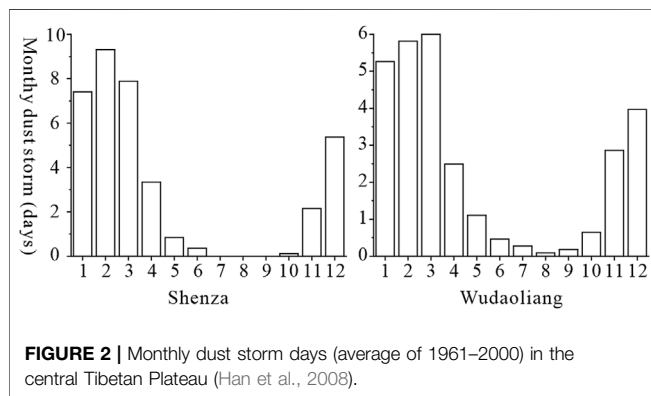
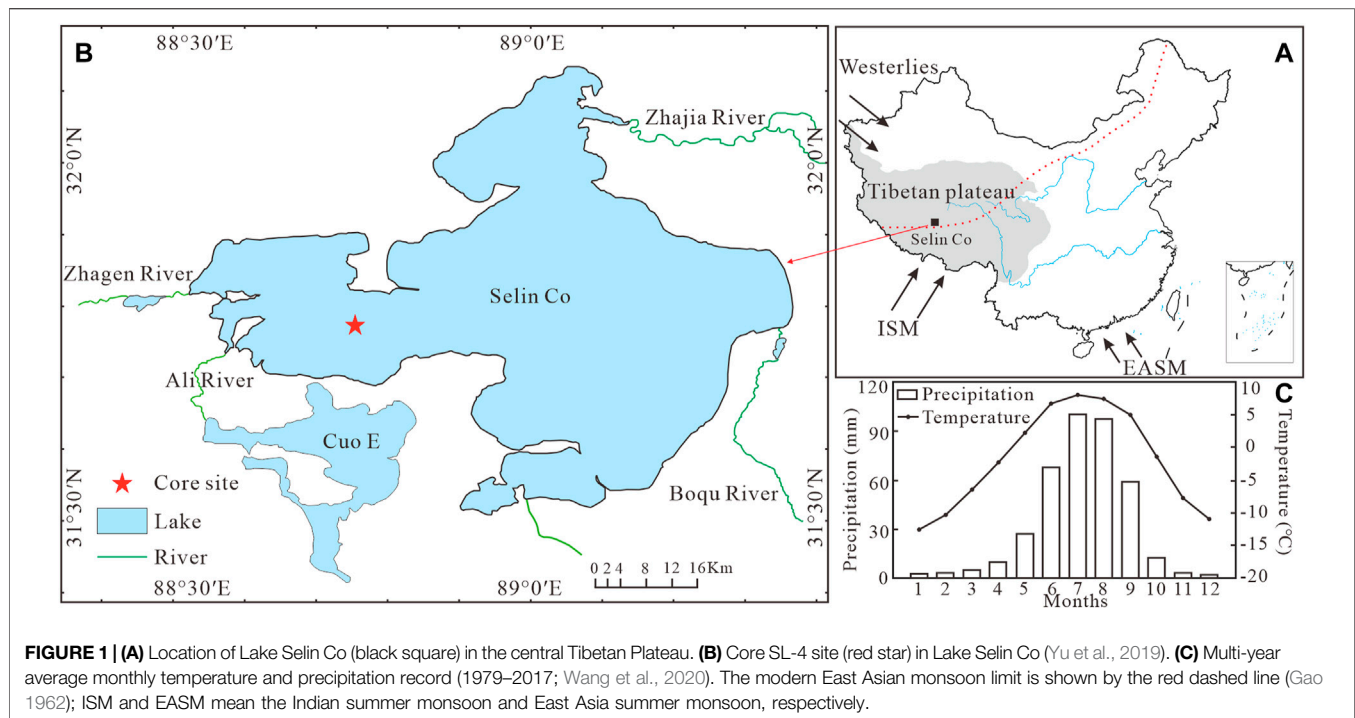
In this article, a 1.79-m lake core from Lake Selin Co has been collected, and the grain size end-member model analysis was applied to the Lake Selin Co sediments since the Late Holocene as well as the aeolian components were identified to reconstruct the past aeolian activity in the central Tibetan Plateau.

2 REGIONAL SETTING

Selin Co is a brackish lake located in the central Tibetan Plateau (88°32′–89°22′E, 31°32′–32°07′N, 4,530 m, above the sea level), about 90 km west of Bange County in Naqu District. The lake consists of two parts. The eastern part has a larger area and has a shallower water body with a maximum water depth of ca. 35 m; the western part is relatively smaller but has a deeper water body (Figure 1; Wang et al., 2019). Lake Selin Co covers a total area of ~3,262 km². The pH value is 9.6, and the salinity is approximately 17.45%. It is a sodium sulfate-type brackish water lake. The total ion concentration in the lake is 11.07 g/L. The cation primarily is Na⁺ with some K⁺, Mg²⁺, and Ca²⁺; the anion primarily is SO₄²⁻ with some Cl⁻, HCO₃⁻, and CO₃²⁻ (Gu et al., 1994; Deji et al., 2018; Wang et al., 2019).

The drainage system is largely developed in the Selin Co catchment, and the main perennial and seasonal rivers are Zhajia River, Zhagen River, Ali River, and Boqu River (Figure 1B; Deji et al., 2018; Wang et al., 2019). The Zhajia River originates in the Tanggula mountains, Geladandong, Jiregepa, and other snow mountains that fill into Lake Selin Co at the north shore of the eastern part. The Zhagen River, an intermittent river with shallow and clear water during the rainy season, originates from the Jiagang snow mountain in the east of Gyaring Co and enters Lake Selin Co from the west shore. The shallower Ali River, a clear seasonal river, infuses the western part of Lake Selin Co. The Boqu River is an intermittent river that originates from the Baburi snow mountain and empties into eastern Lake Selin Co (Wang et al., 2019). The glacier covers an area of around 593 km² or about 1% of the total catchment area of Lake Selin Co (Hou et al., 2021). The Lake Selin Co’s principal supply source is glacial meltwater (Deji et al., 2018; Hou et al., 2021).

The Lake Selin Co region is mainly affected by the Indian summer monsoon and westerlies (Gyawali et al., 2019). According to remote sensing and field observations, Lake Selin Co is typically covered in ice from late December to mid-April of the following year (Kropáček et al., 2013; Zhang et al., 2014; Guo et al., 2016). Annual precipitation ranges between 290 and 321 mm, and the annual evaporation total can reach 2,176 mm. The average annual temperature is 0.8–1.0°C, and the number of annual gale days (i.e., winds >62 kmhr⁻¹) is between 103 and 132 days (Da 2011). Except for May to September, the other months’ mean temperatures in the Lake Selin Co area are below 0°C. Precipitation is the heaviest between



June and September, contributing to 83% of annual precipitation; yet, the basin's multiyear average monthly precipitation is less than 10 mm from November to March (Figure 1C; Wang et al., 2020).

Modern dust storm events in the central Tibetan Plateau are recorded by meteorological stations at Shenza (30°56'N, 88°42'E, 4,680 m) and Wudaoliang (35°12'N, 93°06'E, 4,800 m) and primarily emerge from December to April (1961–2000; Figure 2; Han et al., 2008), owing to the absence of precipitation in the winter and early spring as well as the accompanying high frequency of wind (Bai et al., 2006). Therefore, the dust that falls into Lake Selin Co occurs primarily during the winter (December to April). The main vegetation types are alpine prairie, alpine meadows, and alpine shrubbery (Kou et al., 2021). The *Aytemisia wellby* grassland occupies the lake basin's periphery, while the *Kobresia littledalei*

swampy meadow covers the river shoal and low swampy ground along the shoreline (Sun et al., 1993).

3 MATERIALS AND METHODS

3.1 Core Sampling and Preparation

A total of six lake cores were drilled in the western part of Lake Selin Co at a water depth of 30 m. The longest core measures 2.78 m (Wang and Zheng 2014). A 1.79-m core SL-4 was sliced at 1 cm intervals. For grain size testing, 167 samples were prepared. The upper half of the core is composed primarily of gray-white medium-fine sand or fine silt with an interlayer of black clay, while the lower section is composed primarily of gray-black and black clay with a reasonably fine lithology. Figure 5 illustrates the detailed lithology.

3.2 AMS ^{14}C Age Dating

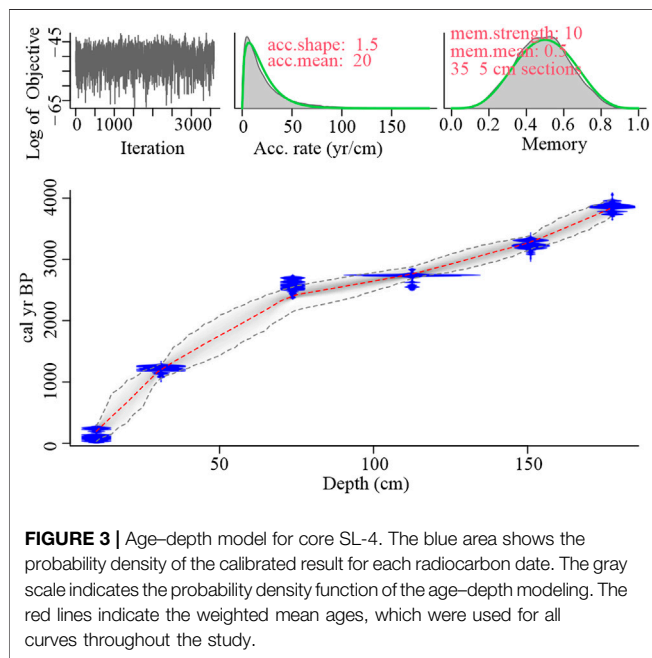
6 AMS ^{14}C was extracted from bulk organic matter samples at the Beta ^{14}C Lab in the United States (Table 1; Figure 3). Calibration of the ^{14}C dates was performed using the IntCal13 calibration curve (Reimer et al., 2013). The age model was established using the Bacon package within the R open-source statistical environment by fitting a polynomial function to the age-depth data (Blaauw and Christen 2011).

3.3 Grain-Size Measurement and End-Member Modeling

To eliminate organic matter and carbonates from subsamples, they were pre-treated by boiling with H_2O_2 (10%) and HCl (10%). The samples were then added to distilled water and left overnight.

TABLE 1 | Radiocarbon ages for samples from cores collected at Lake Selin Co.

Sample ID	BETA Lab ID	Depth (cm)	Dating material	^{14}C age (yr BP)	^{14}C error	RA-corrected ^{14}C age (yr BP)	Calibrated age (yr BP)
SL-4C-1	548798	10	Organic matter	2,370	30	121	197
SL-4C-2	548799	31	Organic matter	3,530	30	1,281	1,202
SL-4C-3	548800	73.75	Organic matter	4,740	30	2,491	2,400
SL-4C-4	548801	112.5	Organic matter	4,850	30	2,601	2,765
SL-4C-5	548802	151	Organic matter	5,280	30	3,031	3,286
SL-4C-6	548803	177.5	Organic matter	5,810	30	3,561	3,844



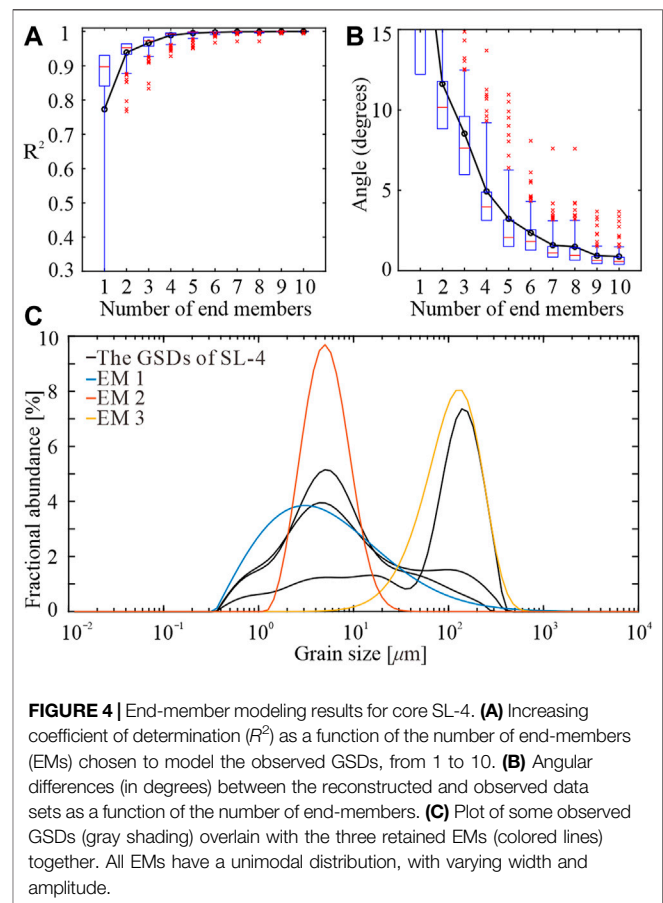
Afterward, the samples were dispersed for 5 min with 10 ml sodium hexametaphosphate on an ultrasonic vibrator to completely disaggregate the particles prior to grain size analysis.

A Malvern Mastersizer 2000 instrument was used to determine the grain size. The range of measurement is 0.02–2000 μm . The repeated measurement error is less than 2%. Then, the samples were inserted into the system using a Hydro MV module. The sample quantity was adjusted to obtain a laser-beam obscuration of between 10 and 20%. The average GSDs for each sample ($n = 167$) were calculated using two repeated measurements and served as the input data for the end-member analysis. The acquired GSDs were unmixed using the MATLAB graphical user interface software program AnalySize.

4 RESULTS

4.1 Chronology

To determine the reservoir effect from the core, the “intercept method” was used (Hou et al., 2012). Zhang et al. (2016) proposed that the regression approach is not restricted to linear types and



introduced quadratic-type regressions. Usually, the regression with the highest correlation (represented by R^2 values) is used to describe the age–depth relationship. In this study, the quadratic relationship gives a higher R^2 value than the linear equation. There is an intercept of 2,249 years BP according to quadratic-type regression ($R^2 = 0.9522$). Wang and Zheng (2014), and Gyawali et al. (2019) calculated the reservoir age to be 1890 and 2,635 years from Lake Selin Co. The inconsistency in the predicted reservoir was probably caused by cores obtained from different locations. However, there are no discernible variations between the reservoir age calculated in this study and the results of earlier investigations. Therefore, the reservoir age in this study was 2,249 years BP.

It was subtracted from all measured ^{14}C ages assuming a constant reservoir age throughout the depth. The reservoir effect-

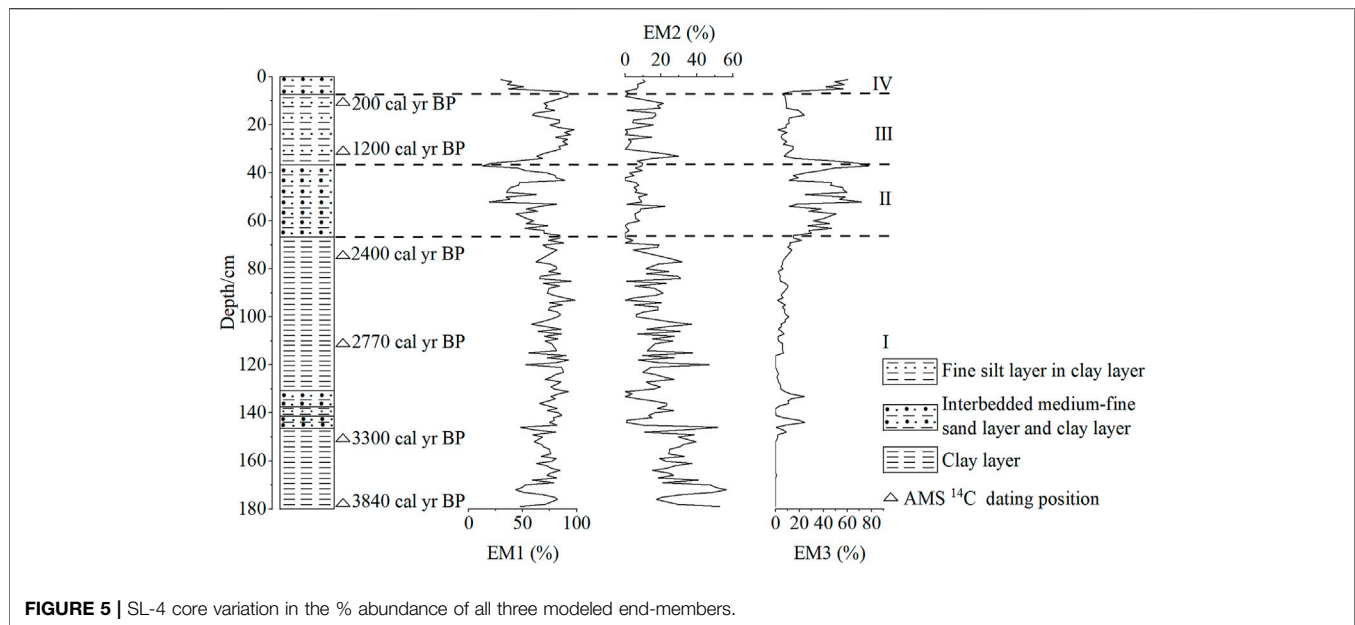


FIGURE 5 | SL-4 core variation in the % abundance of all three modeled end-members.

adjusted chronology was loaded into Bacon software after deducting the reservoir age. A Bayesian accumulation model was used to establish an age–depth model (Figure 3; Blaauw and Christen 2011). At the bottom of the core, the old stage was about 3,900 cal yr BP. The average sedimentation rate is 0.046 cm/yr. The average rate calculated in this study is essentially same as the Gyawali's et al. (2019) average sedimentation rate of 0.045 cm/yr, which is slightly lower than the average sedimentation rate of 0.052 cm/yr calculated by Wang and Zheng (2014).

4.2 Grain Size Results

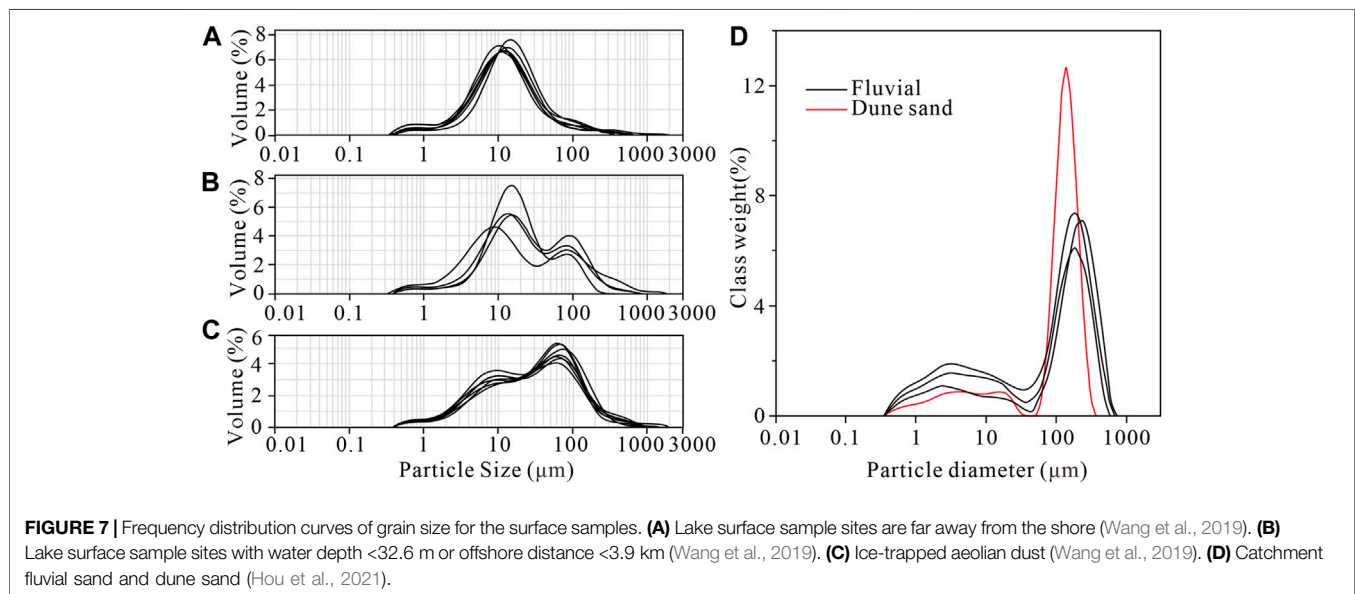
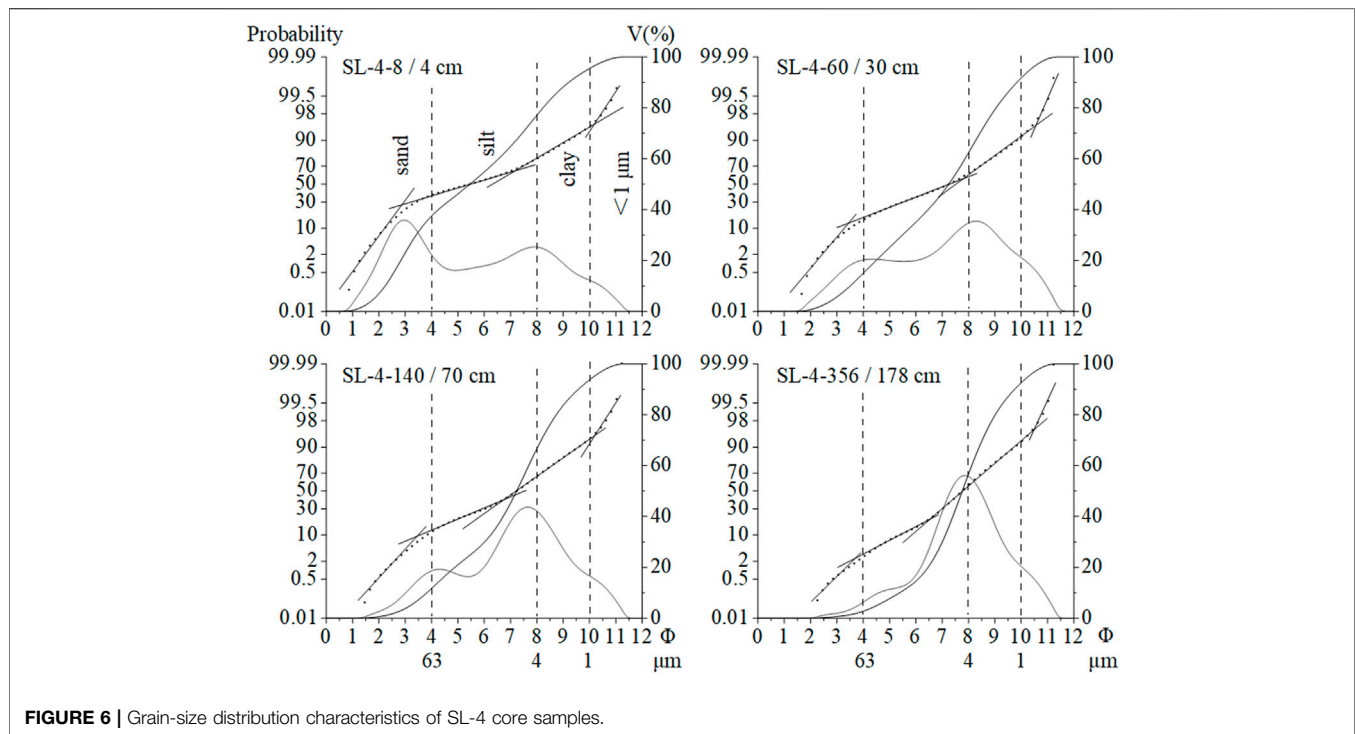
The sediments of Lake Selin Co contain sand, silt, and clay components. However, a polymodal grain-size distribution is revealed when all samples ($n = 167$) are superimposed. Hence, all the GSD data were separated by the AnalySize program, and the minimum number of end-members (EMs) required is also determined based on the calculated coefficient of determinations (R^2) and angular deviation (Paterson and Heslop 2015). As the number of EMs increases, the goodness-of-fit statistics show an increasing fit (higher R^2) to the raw GSDs spectra (Figure 4A). According to Figures 4A,B, the third end-member represents a critical position in terms of linear correlations and angular deviation. Therefore, the three end-members fit in minimum EMs with relatively high R^2 . So, we chose a three-EM model to depict the particle sources and deposition process in Lake Selin Co since the Late Holocene. The end-member modal sizes are 2.9 μm (EM1), 5 μm (EM2), and 138 μm (EM3; Figure 4C).

The percentage contents of these three modeled end-members are shown in Figure 5. EM1 is the most abundant particle fraction throughout the whole core and is highly varied, ranging from ~12.9 to ~98.4%. The relative abundance of EM2 varies between 0 and ~56.3%. EM3 ranges from 0 to ~77.7%, with very low percentages throughout the core and moderately high

percentages outside at some intervals (e.g., 76–38 cm, 148–125 cm, and 7–0 cm).

The grain size changes in the SL-4 core sediments are classified into four stages: 179–76 cm, 76–38 cm, 38–7 cm, and greater than 7 cm (Figure 5). Between 179 and 76 cm (stage I), the proportions of EM1, EM2, and EM3 are 43.7–98.4%, 0–56.3%, and 0–24.1%, respectively, with 74.6, 21.3, and 4.0% as the corresponding averages. From 76 to 38 cm (stage II), the EM1 ranges from 18.9 to 88.9% with an average of 61%, EM2 ranges from 0 to 22.1% with an average of 6.0%, and EM3 ranges from 7.1 to 71.8% with an average of 33%. Between 38 and 7 cm (stage III), the proportions of EM1, EM2, and EM3 range from 12.9 to 97.9% (average 74.2%), 0–29.7% (average 9.4%), and 2.1–77.7% (average 16.4%), respectively. Above 7 cm (stage IV), the proportions of EM1, EM2, and EM3 range from 29.7 to 85.5% (average 46.4%), 0–11.1% (average 6.9%), and 14.5–60.5% (average 46.7%), respectively.

To better understand the sediment constitution and deposition processes, we selected four representative samples from stage I to IV and plotted their cumulative curves, probability cumulative curves, and distribution curves in the same coordinates, as shown in Figure 6. The probability cumulative curves for all four samples indicate a four-stage type, and the grain size range varies greatly (~0.2–354 μm ; Figure 6). The fraction of rolling load is between 2 and 25%. The sand is the main component with a grain size range varying from 88 to 354 μm . The grain size range of the saltation load varies between 0.7 and 88 μm , with silt and clay as the main components of the load and less sand with a broad peak span. The cutoff point of the two saltation loads is between 6 and 11 μm . The suspension load is approximately 10%, with a high slope, medium-good sorting, and grain size ranging from 0.2 to 1 μm , dominated by clay. The cutoff point between the rolling and saltation load is coarse and ranges between 88 and 125 μm , while the cutoff point between the saltation and suspension loads is fine and near 1 μm .



5 DISCUSSION

5.1 Environmental Significance Interpretation of Obtained EMs

Clastic particles were deposited at the lake bottom principally via three transport paths, according to Wang et al. (2019): river or runoff, wind (frequently trapped by ice in winter, deposited following ice melting in summer and autumn), and long-term suspension maintained by wave action. The key components of

the sediments, as illustrated in Figure 6, are the saltation and suspension load. The multi-peak patterns of grain-size distribution curves in the Lake Selin Co deposition processes show complicated sedimentary provenance, medium, and hydrodynamic circumstances (Figure 6). Furthermore, the end-member modeling results reflect that the deposition of clastic particles is influenced by multiple transport-deposition processes from the perspective of sedimentation dynamics. We analyzed the grain-size distribution of Lake Selin Co surface

sediment and modern aeolian dust trapped on the ice, fluvial sand, and aeolian sand dunes around the lake to determine the composition of the source material for the Lake Selin Co sediment (Figure 7).

With a modal grain size of $\sim 2.9 \mu\text{m}$, EM1 represents the finest particle fraction in Lake Selin Co sediments (Figure 4C). This super-microparticle clay EM1 in lake sediment represents a long-term suspension fraction in standing water (Dietze et al., 2012; Xiao et al., 2013; Liu et al., 2016) and settles under calm conditions (Dietze et al., 2014).

From nearshore to offshore, the fine particle content increases while the coarse particle content decreases, implying that hydrodynamic sorting is taking place (Figure 7A,B; Wang et al., 2019). We assume that the flows from the river/runoff were not strong enough to transport coarse particles to the center of the lake, whilst those flows could possibly transport finer sediments to deep water. The fine particles suspended in the current and deposited in the lake water is at a standstill (Qiang et al., 2007). Additionally, when the precipitation or glacial meltwater increases, a large amount of water can raise lake levels, yet a deeper lake can deposit finer particles below weak hydrodynamics wave-base (Hou et al., 2021). A fine silt end-member has been detected in the lake on the Tibetan plateau, which has been interpreted as the sediment settling from river/runoff processes (Ma et al., 2019; Zhang et al., 2021). The mud-silt component, mainly fine particles, is represented by EM2, which has a modal size of $5 \mu\text{m}$. Therefore, EM2 instructs a fine particle fraction by the river/runoff inputting to the lake.

The modal size of EM3 is approximately $138 \mu\text{m}$, which represents the sand fraction. The grain-size distribution of the sediments could be affected by variations in the distance between the inflow and the deposition location as a result of lake-level fluctuations (Wang et al., 2021). The lake center (i.e., core site) may be far from the lake shore during periods of high lake level; the sediment/water interface is usually less disturbed by river/runoff inflow and wave action; and coarse particles transported by the river/runoff are difficult to reach the core location, resulting in fine particles deposited in the sediment center (Kasper et al., 2012; Bird et al., 2014). Moreover, the mode size of the fluvial sand found in the sample sites around Lake Selin Co ranges from 181 to $209 \mu\text{m}$ (Figure 7D; Hou et al., 2021). Single-frequency distribution curves without coarser modal size at 181 and $209 \mu\text{m}$ are recorded from the sediments of the lake surface sample sites with a large distance from the shore (Figure 7A). It indicates that the coarse particles of sediments at the core location are relatively unaffected by the river/runoff. In regions with less precipitation, fluvial sediment fractions $>60 \mu\text{m}$ are difficult to be transported to the sedimentary center of the lake with high lake level and large surface (Deckker et al., 1991). Furthermore, when the core site is close to the river/runoff inflow and the lake level is low, the core site is likely to receive more coarse-grained material delivered by the river/runoff.

Meanwhile, the wind can also transfer coarse material to Lake Selin Co. Wind frequently transports coarse particles to the center of high-sand-content lakes in Northwest China's arid and semiarid regions (Chen et al., 2013; Zhang et al., 2021). The

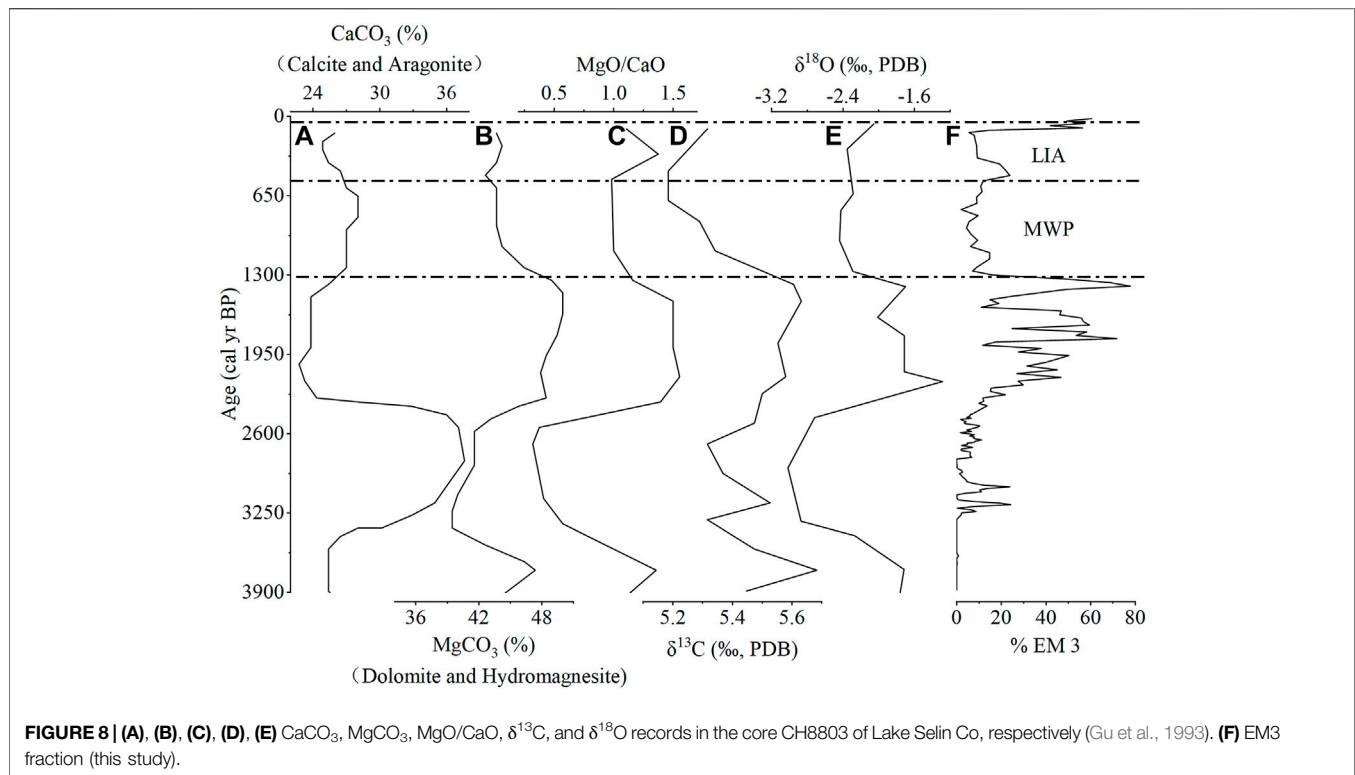
size distribution curves of ice-trapped aeolian dust grains from Lake Selin Co show coarser aeolian components with a modal size of roughly $\sim 70 \mu\text{m}$ (Figure 7C). The EM3 component grain-size distribution interval contains the modal size of ice-trapped aeolian dust, indicating that the grain size of about $70 \mu\text{m}$ in the core represents an aeolian fraction. Additionally, the grain-size distribution curve of aeolian dune sand distributed on the lake beach of Lake Selin Co reveals that it is mainly made up of fine to medium sand with a modal size of $140 \mu\text{m}$ (Figure 7D). It agrees with the EM3 fraction's modal size, indicating that coarser particles were driven into the lake during a sand storm with strong winds. Regardless of the lake level, coarse particles can be deposited directly into Lake Selin Co through sand storms or freeze on the lake ice-layer in winter and subsequently sink into the lake owing to ice melting. As a result, the EM3 fraction contains inputs from both aeolian and river/runoff sources. To some extent, variations in the EM3 fraction content can signal changes in aeolian activity. When the EM3 fraction content is low, aeolian activity is weaker, and the lake level is higher; contrariwise, the high EM3 fraction indicates stronger aeolian activity and low lake level.

5.2 Aeolian Activity History During the Last 3,900 years Inferred From Grain-Size Spectra

Climate change has a great impact on the aeolian activity (Yang et al., 2007; Wolfe 2021). The abundance of magnesium-rich authigenic carbonate minerals (dolomite and hydromagnesite) in the Lake Selin Co sediments indicates that the degree of aridity of the climate intensified as the MgO/CaO ratio and MgCO_3 concentration increased (Gu et al., 1993). The authigenic carbonate consisting of calcite and aragonite that was deposited, with an increase in CaCO_3 content and a drop in the MgO/CaO ratio, reflects a warmer and wetter climatic environment (Gu et al., 1993). A dry and cold climate is indicated by higher $\delta^{18}\text{O}$ values in authigenic carbonate (Gu et al., 1993). In the Late Holocene, the Selin Co regional climate evolved oscillatively to cold and dry, which was compatible with records from the central Tibetan Plateau's lakes of Zigetang Co, Taro Co, and Nam Co (Gu et al., 1993; Herzsuh et al., 2006; Cheung et al., 2014; Laug et al., 2021).

The aeolian activity history in the Selin Co region over the last 3,900 years can be reconstructed based on the component EM3 (Figure 8F). According to the variation of EM3 component content, the significant aeolian activity periods in the central Tibetan Plateau were inferred from 3,200 to 2,900 cal yr BP, 2,400–1,400 cal yr BP, and after 130 cal yr BP. A lower frequency and weaker intensity of aeolian activity were recorded from the other periods. Comparing the climate change characteristics of the study area, we suggest that most periods of low aeolian activity correspond to the humid conditions, probably due to the wet climate that reduced the intensity of aeolian activity to some extent (Yang et al., 2007).

The climate of Lake Selin Co was dry and cold at 3,900–3,400 cal yr BP, according to Gu et al. (1993) and Gyawali et al. (2019) studies, with decreased MgCO_3 , $\text{MgO}/$



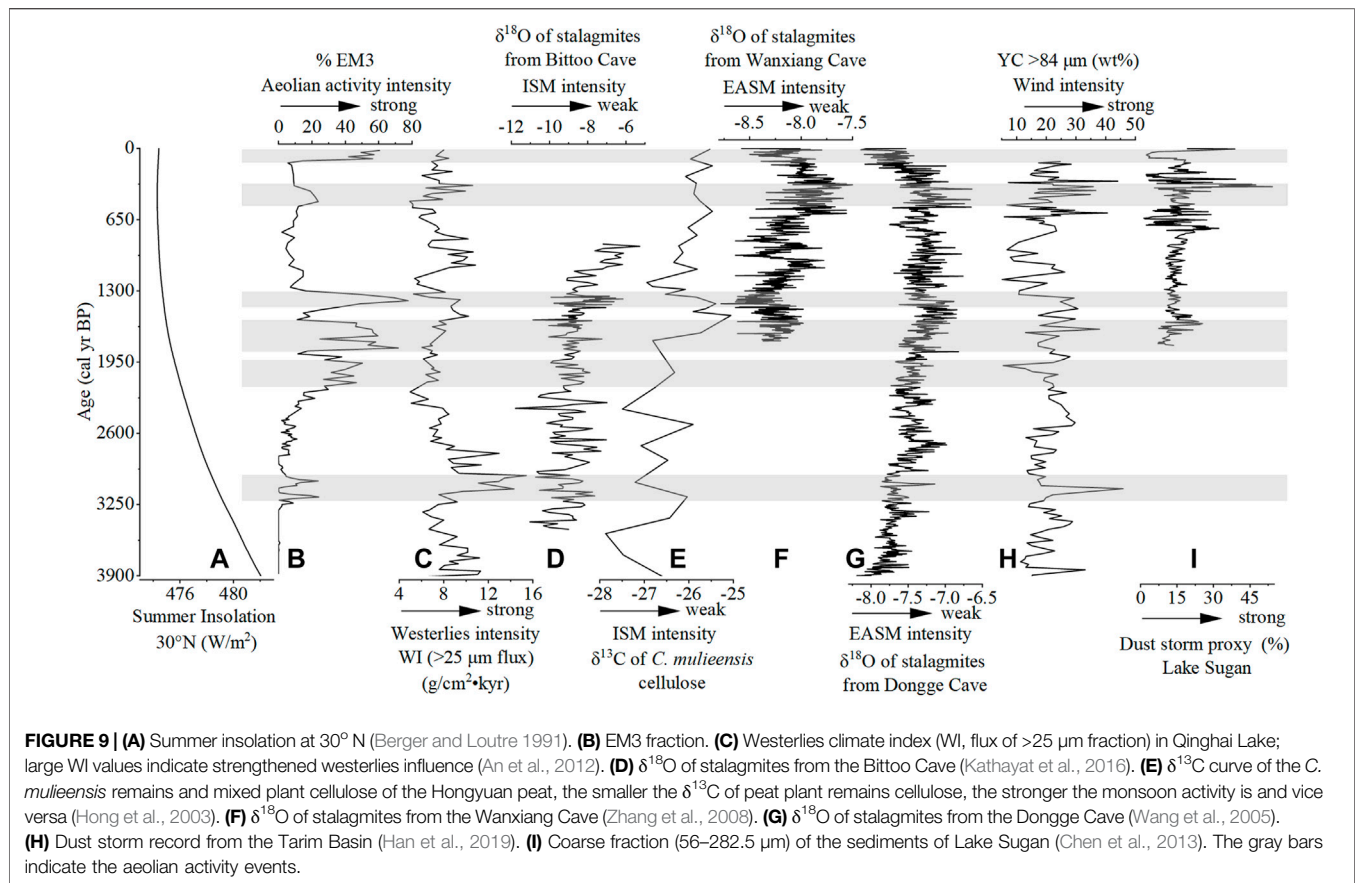
CaO, and δ¹⁸O values (**Figures 8B,C,E**). The aeolian activity was not developed in this period. It indicates that the climate changed from dry and cold to warm and wet, and the intensity of the dry and cold climate was not too strong. The better conditions were probably favorable to the vegetation so that to restrain aeolian activity.

The climate was relatively wet from 3,400 to 2,400 cal yr BP (**Figure 8**; Gu et al., 1993), and wet conditions were recorded from Nam Co and Tangra Yumco at 3,400–2,300 cal yr BP (Kasper et al., 2012; Ma et al., 2020). The frequency of aeolian activity was low, and the intensity was weak during this period. Aeolian activity peaked between 3,200 and 2,900 cal yr BP, owing to a regional climatic shift associated with the 2.8 ka BP cold event (~3,300–2,800 cal yr BP; Sun et al., 2020). This occurrence was witnessed in several parts of the Tibetan Plateau, i.e., lakes Ngamring Co and Qinghai as well as the Hongyuan peatland (Yu et al., 2006; Hou et al., 2016; Sun et al., 2020).

The climate was cold and dry at 2,400–1,400 cal yr BP (**Figure 8**; Gu et al., 1993). Dry conditions were inferred from lakes Nam Co and Tangra Yumco at 2,300–1,700 cal yr BP (Kasper et al., 2012; Ma et al., 2020). Changes in δ¹⁸O and δ¹³C values of carbonate fluctuated significantly with the peak at 2,400–1,400 cal yr BP (**Figures 8D,E**). It signifies a dramatic evaporation event caused by the cold and dry climate, resulting in a drop at the lake level (Gu et al., 1993; Morinaga et al., 1993; Xue et al., 2010). Another factor that could have caused the lake level to drop was the weakening of the monsoon, which resulted in less precipitation (Gu et al., 1994; Shi et al., 2017;

Hou et al., 2021). Simultaneously, during the low lake level, the EM3 proportion was high, indicating intense aeolian activity. Therefore, in cold and dry conditions, coarse particles may be transported by wind and, to a lesser extent, by the river/runoff. With the lake-level lowering, the core site is close to shallow nearshore, so that coarse particles deposited were carried by the river/runoff. The aeolian activity estimated from this study is compatible with the record of strong aeolian activity from the Dinggye area in the southern Tibetan Plateau between 2000 and 1,100 cal yr BP (Pan et al., 2014). The differences in dates are probably from the shorter paleo-aeolian sedimentary sequence and lower chronological resolution (Pan et al., 2014). The cold and dry climatic conditions provide a background for aeolian activity during this period (Yang et al., 2007). Under dry conditions, the effective humidity decreased and vegetation cover and soil consolidation became bad, resulting in increased sand sources and dust release; meanwhile, the cooling process was accompanied by windy weather, increasing the possibility of aeolian activity by providing the necessary dynamical effect (Yang et al., 2007; Ma et al., 2016).

The humidity slightly increased after 1,400 cal yr BP (**Figure 8**; Gu et al., 1993), and the Medieval Warm Period (MWP) arrived. The content of the EM3 fraction reduced considerably with a weak aeolian activity during the MWP. The warm and humid climate favored vegetation in the region to inhibit aeolian activity. Following then, aeolian activity increased in frequency and intensity throughout the Little Ice Age (LIA). In such a frigid climatic background, the



study area provided suitable dynamical conditions, giving enhanced source material and wind power for the aeolian dust transport (Yang et al., 2007; Ma et al., 2016). Aeolian activity appeared at 350–550 cal yr BP and after 130 cal yr BP. It is well consistent with the high dust events record from the Malan ice core for nearly 800 years (Wang et al., 2006). This study's findings on aeolian activity during the LIA are congruent with ice core records from the Tibetan Plateau. During 1800–2000 AD, increased dust concentrations were recorded from the Dasuopu ice core in the Tibetan Plateau's southern region (Thompson et al., 2000). The Guliya ice core was used to infer the significant dust peak phases between 1770 and 1900 AD (Yang et al., 2007). At 1860–1874 AD and 1930–1954 AD, the Tanggula ice core recorded a strong dust flux (Wu et al., 2013).

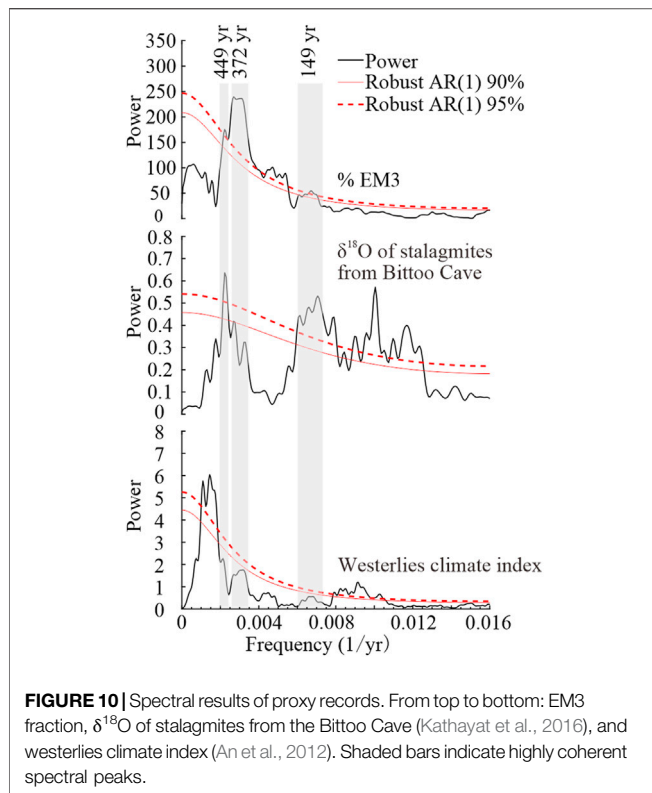
5.3 Regional Comparison

The aeolian activity archives in this study show that aeolian activity was more prevalent during cold and dry periods. The records from Chen et al. (2013) and Qiang et al. (2014) support this theory. Summer insolation in the Northern Hemisphere has been decreasing from 3,900 cal years BP, indicating a cooling trend (Figure 9A; Berger and Loutre 1991). As a result, in the context of cooling, the probability and intensity of cold air intrusion increase, and the frequent

occurrence of windy weather creates better dynamical conditions for sustained aeolian activity (Yang et al., 2007; Wolfe 2021). In order to better illustrate the factors impacting the aeolian activity in the central Tibetan Plateau, the aeolian activity record is therefore compared with regional paleoclimatic records (Figure 9).

Figures 9B,H,I show the aeolian activity records of Lake Selin Co in the central Tibetan Plateau, Yang Chang (YC) section in the southern margin of the Tarim Basin, and Suga Lake in the Qaidam Basin in the northern Tibetan Plateau, respectively. Compared with the Suga Lake record, large differences in the history of aeolian activity are presented in the two areas (Figures 9B,I). Sand storms came into being and intensified during 300–500 AD, 1180–1,240 AD, and 1500–1700 AD in the Suga Lake region in the last 2000 years (Chen et al., 2013). Whilst the aeolian activity events in the Lake Selin Co are well consistent with the YC section record, but there are some slight differences between them (Figures 9B,H). The difference between age and aeolian activity history implies that the three regions have different main regulating forces.

The aeolian activity in the Suga Lake region coincided with the intensification of Siberian high, resulting in frequent incursions of cold air masses from higher latitudes into the dust source area in northwestern China (Chen et al., 2013).



The aeolian activity in the Tarim Basin is influenced not only by changes in solar activity but also by increased low level wind strength and delayed transition of seasonal jet due to enhanced and southward shifts of the westerly jet during cold periods (Han et al., 2019). The central Tibetan Plateau's aeolian activity was compared to Indian summer monsoon (ISM) and westerlies records. We assume that the period of strong aeolian activity in the research area generally coincides with the weakening of the ISM and the strengthening of the westerlies (Figures 9B–E). Meanwhile, the spectral analyses of the aeolian activity record of Lake Selin Co, the ISM, and the westerlies present consistent dominating cycles centered at ~149 years, ~372, and ~449 years (Figure 10). This further corroborates the relationship between aeolian activity changes in the central Tibetan Plateau with the ISM and the westerlies changes. However, the three dominant cycles are not evident in the westerlies spectrum. It seems likely that the westerlies are not a direct cause of the variation of aeolian activity in the study area. The westerlies influence aeolian activity in both the central Tibetan Plateau and the Tarim Basin. However, the controlling role of the westerlies in the formation of aeolian activity in the Tarim Basin was probably stronger than that in the central Tibetan Plateau region. With the comparison of the $\delta^{18}\text{O}$ records from stalagmites in Wanxiang and Dongge caves, aeolian activity in the central Tibetan Plateau usually corresponded to the strengthened East Asian summer monsoon periods (Figures 9B,F,G). Correlation analysis with $\delta^{18}\text{O}$ data of stalagmites from the Wanxiang Cave

($R = -0.29$ with $p < 0.01$) and Dongge Cave ($R = -0.41$ with $p < 0.01$) presents a moderate negative correlation. This indicates that the East Asian summer monsoon has a limited impact on aeolian activity in the central Tibetan Plateau. It supports the earlier hypothesis that the ISM and the westerlies have the greatest influence on the climate of the central Tibetan Plateau (Wang et al., 2017; Gyawali et al., 2019; Hou et al., 2021).

The comparison reveals that ISM-dominated regional humidity may play a key role in regulating the study area's dust emission and aeolian accumulation. When the ISM intensity drops, less precipitation falls in the Lake Selin Co area, resulting in low effective humidity, sparse vegetation cover, and easily mobilized ground surface particles. Moreover, as the westerlies strengthen, the relatively bare ground surface becomes more prone to raise coarser dust particles as a result of vigorous wind erosion. The air masses associated with the ISM only need to cross a small section of the Indian subcontinent before reaching the Tibetan Plateau from the south, but the westerlies must cross the majority of the Eurasian continent before reaching the Tibetan Plateau region. These two paths differ not only in terms of their overall source regions but also in terms of the distances they travel to water sources (oceans; Zhu et al., 2015). Therefore, the transfer of moisture differs between these two atmospheric circulation systems, with the westerlies bringing minimal moisture to the Tibetan Plateau and the ISM bringing a high amount of precipitation (Zhu et al., 2015). Because the study location is located at a high altitude on the central Tibetan Plateau, dry westerlies may only slightly improve humidity in the study area when the westerlies are enhanced (Zhu et al., 2015). As a result, enhancing westerlies across the central Tibetan Plateau may promote aeolian activity. Our findings match the reconstructed aeolian activity history from the Dinggye area in the southern Tibetan Plateau since 3,900 cal yr BP within the error range of chronology dating (Pan et al., 2014). The ISM circulation likely has a significant impact on both areas. Atmospheric circulation disturbances influence aeolian activity, with various driving mechanisms controlled by different atmospheric circulation systems. The development of aeolian activity in the central Tibetan Plateau is influenced by regional humidity, which is dominated by ISM.

6 CONCLUSION

The grain size end-member modeling of the Lake Selin Co's SL-4 core gives important independent information about changes in aeolian activity in the central Tibetan Plateau since 3,900 cal yr BP. The observed GSDs are subdivided into statistically robust EMs, each of which is associated with a distinct source region and transport process, i.e., long-term suspension component sources (EM1), fine catchment river/runoff sources (EM2), and coarse fraction from aeolian and river/runoff sources (EM3). The temporal variation in EM3-relative abundance is proposed to be a

valuable indicator of aeolian activity over the central Tibetan Plateau. Remarkable aeolian activity occurred during 3,200–2,900 cal yr BP, 2,400–1,400 cal yr BP, and after 130 cal yr BP. According to the study's findings, dry and cold climate conditions favor aeolian activity. Additionally, aeolian activity in the central Tibetan Plateau was directly related to solar insolation. Since 3,900 cal yr BP, aeolian activity in the central Tibetan Plateau had been formed under conditions that resulted in the Indian summer monsoon weakening and the westerlies strengthening compared with other proxies.

DATA AVAILABILITY STATEMENT

The original contributions presented in the study are included in the article/Supplementary Material, further inquiries can be directed to the corresponding author.

REFERENCES

- An, C.-B., Zhao, J., Tao, S., Lv, Y., Dong, W., Li, H., et al. (2011). Dust Variation Recorded by Lacustrine Sediments from Arid Central Asia since ~ 15 Cal Ka BP and its Implication for Atmospheric Circulation. *Quat. Res.* 75 (3), 566–573. doi:10.1016/j.yqres.2010.12.015
- An, Z., Colman, S. M., Zhou, W., Li, X., Brown, E. T., Jull, A. J. T., et al. (2012). Interplay between the Westerlies and Asian Monsoon Recorded in Lake Qinghai Sediments since 32 Ka. *Sci. Rep.* 2, 619. doi:10.1038/srep00619
- Bai, H. Z., Ma, Z. F., Dong, W. J., Li, D. L., Fang, F., and Liu, D. X. (2006). Climatic Properties and Sandstorm Causes in Tibet Plateau. *J. Desert Res.* (02), 249–253. doi:10.3321/j.issn:1000-694X.2006.02.016
- Berger, A., and Loutre, M. F. (1991). Insolation Values for the Climate of the Last 10 Million Years. *Quat. Sci. Rev.* 10 (4), 297–317. doi:10.1016/0277-3791(91)90033-Q
- Bird, B. W., Polisar, P. J., Lei, Y., Thompson, L. G., Yao, T., Finney, B. P., et al. (2014). A Tibetan lake Sediment Record of Holocene Indian Summer Monsoon Variability. *Earth Planet. Sci. Lett.* 399, 92–102. doi:10.1016/j.epsl.2014.05.017
- Blaauw, M., and Christen, J. A. (2011). Flexible Paleoclimate Age-Depth Models Using an Autoregressive Gamma Process. *Bayesian Anal.* 6 (3), 457–474. doi:10.1214/ba/1339616472
- Chen, F., Qiang, M., Zhou, A., Xiao, S., Chen, J., and Sun, D. (2013). A 2000-year Dust Storm Record from Lake Sugin in the Dust Source Area of Arid China. *J. Geophys. Res. Atmos.* 118 (5), 2149–2160. doi:10.1002/jgrd.50140
- Cheung, M. C., Zong, Y., Zheng, Z., Huang, K., and Aitchison, J. C. (2014). A Stable Mid-late Holocene Monsoon Climate of the central Tibetan Plateau Indicated by a Pollen Record. *Quat. Int.* 333, 40–48. doi:10.1016/j.quaint.2014.03.010
- Da, S. (2011). The Trends of Air Temperature and Precipitation Changes the Past 50 Years in Selin Co Lake Area, Tibet. *Tibet Sci. Tech.* 36 (01), 42–45. (in Chinese). doi:10.3969/j.issn.1004-3403.2011.01.021
- Deckker, P., Corregge, T., and Head, J. (1991). Late Pleistocene Record of Cyclic Eolian Activity from Tropical Australia Suggesting the Younger Dryas Is Not an Unusual Climatic Event. *Geology*, 19, 602. doi:10.1130/0091-7613(1991)019<0602:lproce>2.3.co;2
- DeJi, Y. Z., NiMa, J., QiangBa, Q. Z., Zeng, L., and LuoSang, Q. Z. (2018). Lake Area Variation of Selin Tso in 1975–2016 and its Influential Factors. *Plateau Mountain Meteorology Res.* 38 (02), 35–41+96. (in Chinese with English abstract). doi:10.3969/j.issn.1674-2184.2018.02.006
- Dietze, E., Hartmann, K., Diekmann, B., Ijmker, J., Lehmkuhl, F., Opitz, S., et al. (2012). An End-Member Algorithm for Deciphering Modern Detrital Processes from lake Sediments of Lake Donggi Cona, NE Tibetan Plateau, China. *Sediment. Geology.* 243–244, 169–180. doi:10.1016/j.sedgeo.2011.09.014

AUTHOR CONTRIBUTIONS

CZ participated in the whole work and drafting of the manuscript; WZ, YL, and CZ contributed to perception and design and final approval of the version to be published; JY, RW, XH, and HL contributed to data analysis.

FUNDING

This study was supported by the fund from the National Natural Science Foundation of China (Grant NSFC 41571177, 41601187, and 41872146), the Fundamental Research Funds for the Central Universities, Lanzhou University (lzujbky-2019–46), and the Foundation of Key Laboratory of Mineral Resources in Western China (Gansu Province), Lanzhou University, and the Second Tibetan Plateau Scientific Expedition and Research (STEP) program (2019QZKK0704).

- Dietze, E., Maussion, F., Ahlborn, M., Diekmann, B., Hartmann, K., Henkel, K., et al. (2014). Sediment Transport Processes across the Tibetan Plateau Inferred from Robust Grain-Size End Members in lake Sediments. *Clim. Past* 10 (1), 91–106. doi:10.5194/cp-10-91-2014
- Dong, Z., Brahney, J., Kang, S., Elser, J., Wei, T., Jiao, X., et al. (2020). Aeolian Dust Transport, Cycle and Influences in High-Elevation Cryosphere of the Tibetan Plateau Region: New Evidences from alpine Snow and Ice. *Earth-Science Rev.* 211, 103408. doi:10.1016/j.earscirev.2020.103408
- Esmaili, N., Gharagzloo, M., Rezaei, A., and Grunig, G. (2014). Dust Events, Pulmonary Diseases and Immune System. *Am. J. Clin. Exp. Immunol.* 3 (1), 20–29.
- Gao, Y. X. (1962). “On Some Problems of Asian Monsoon,” in *Some Questions about the East Asian Monsoon*. Editor Y. X. Gao (Beijing: Chinese Science Press), 1–49. (in Chinese).
- Gu, Z. Y., Liu, J. Q., Yuan, B. Y., Liu, D. S., Liu, R. M., Liu, Y., et al. (1993). Monsoon Variations of the Qinghai-Xizang Plateau during the Last 12,000 Years - Geochemical Evidence from the Sediments in the Siling Lake. *Chin. Sci. Bull.* 38 (7), 577–581. (in Chinese). doi:10.1126/science.260.5104.109
- Gu, Z. Y., Liu, J. Q., Yuan, B. Y., Liu, D. S., and Zhang, G. Y. (1994). Lacustrine Authigenic Deposition Expressive of Environment and the Sediment Record from Siling Co, XiZang (Tibet), China. *Quat. Sci.* (02), 162–174. (in Chinese with English abstract).
- Guo, Y., Zhang, Y., Ma, N., Song, H., and Gao, H. (2016). Quantifying Surface Energy Fluxes and Evaporation over a Significant Expanding Endorheic Lake in the Central Tibetan Plateau. *J. Meteorol. Soc. Jpn.* 94 (5), 453–465. doi:10.2151/jmsj.2016-023
- Gyawali, A. R., Wang, J., Ma, Q., Wang, Y., Xu, T., Guo, Y., et al. (2019). Paleoenvironmental Change since the Late Glacial Inferred from Lacustrine Sediment in Selin Co, central Tibet. *Palaeogeogr. Palaeoclimatol. Palaeoecol.* 516, 101–112. doi:10.1016/j.palaeo.2018.11.033
- Han, W., Lü, S., Appel, E., Berger, A., Madsen, D., Vandenberghe, J., et al. (2019). Dust Storm Outbreak in Central Asia after ~3.5 Kyr BP. *Geophys. Res. Lett.* 46 (13), 7624–7633. doi:10.1029/2018GL081795
- Han, Y., Fang, X., Kang, S., Wang, H., and Kang, F. (2008). Shifts of Dust Source Regions over central Asia and the Tibetan Plateau: Connections with the Arctic Oscillation and the westerly Jet. *Atmos. Environ.* 42, 2358–2368. doi:10.1016/j.atmosenv.2007.12.025
- Herzschuh, U., Winter, K., Wünnemann, B., and Li, S. (2006). A General Cooling Trend on the central Tibetan Plateau throughout the Holocene Recorded by the Lake Zigetang Pollen Spectra. *Quat. Int.* 154–155, 113–121. doi:10.1016/j.quaint.2006.02.005
- Hong, Y. T., Hong, B., Lin, Q. H., Zhu, Y. X., Shibata, Y., Hirota, M., et al. (2003). Correlation between Indian Ocean Summer Monsoon and North Atlantic

- Climate during the Holocene. *Earth Planet. Sci. Lett.* 211 (3-4), 371–380. doi:10.1016/S0012-821x(03)00207-3
- Hou, J., D'Andrea, W. J., and Liu, Z. (2012). The Influence of 14C Reservoir Age on Interpretation of Paleolimnological Records from the Tibetan Plateau. *Quat. Sci. Rev.* 48, 67–79. doi:10.1016/j.quascirev.2012.06.008
- Hou, J., Huang, Y., Zhao, J., Liu, Z., Colman, S., and An, Z. (2016). Large Holocene Summer Temperature Oscillations and Impact on the Peopling of the Northeastern Tibetan Plateau. *Geophys. Res. Lett.* 43 (3), 1323–1330. doi:10.1002/2015gl067317
- Hou, Y., Long, H., Shen, J., and Gao, L. (2021). Holocene lake-level Fluctuations of Selin Co on the central Tibetan Plateau: Regulated by Monsoonal Precipitation or Meltwater? *Quat. Sci. Rev.* 261, 106919. doi:10.1016/j.quascirev.2021.106919
- Kashiwaya, K., Masuzawa, T., Morinaga, H., Yaskawa, K., Baoyin, Y., Jiaqi, L., et al. (1995). Changes in Hydrological Conditions in the central Qing-Zang (Tibetan) Plateau Inferred from lake Bottom Sediments. *Earth Planet. Sci. Lett.* 135 (1), 31–39. doi:10.1016/0012-821X(95)00136-Z
- Kasper, T., Haberzettl, T., Doberschütz, S., Daut, G., Wang, J., Zhu, L., et al. (2012). Indian Ocean Summer Monsoon (IOSM)-dynamics within the Past 4 Ka Recorded in the Sediments of Lake Nam Co, central Tibetan Plateau (China). *Quat. Sci. Rev.* 39, 73–85. doi:10.1016/j.quascirev.2012.02.011
- Kathayat, G., Cheng, H., Sinha, A., Spötl, C., Edwards, R. L., Zhang, H., et al. (2016). Indian Monsoon Variability on Millennial-Orbital Timescales. *Sci. Rep.* 6, 24374. doi:10.1038/srep24374
- Kou, Q., Lin, X., Wang, J., Yu, S., Kai, J., Laug, A., et al. (2021). Spatial Distribution of N-Alkanes in Surface Sediments of Selin Co Lake, central Tibetan Plateau, China. *J. Paleolimnol.* 65 (1), 53–67. doi:10.1007/s10933-020-00148-8
- Kropáček, J., Maussion, F., Chen, F., Hoerz, S., and Hochschild, V. (2013). Analysis of Ice Phenology of Lakes on the Tibetan Plateau from MODIS Data. *The Cryosphere* 7, 287–301. doi:10.5194/tc-7-287-2013
- Laug, A., Haberzettl, T., Pannes, A., Schwarz, A., Turner, F., Wang, J., et al. (2021). Holocene Paleoenvironmental Change Inferred from Two Sediment Cores Collected in the Tibetan lake Taro Co. *J. Paleolimnol.* 66, 171–186. doi:10.1007/s10933-021-00198-6
- Liu, X., Vandenberghe, J., An, Z., Li, Y., Jin, Z., Dong, J., et al. (2016). Grain Size of Lake Qinghai Sediments: Implications for Riverine Input and Holocene Monsoon Variability. *Palaeogeogr. Palaeoclimatol. Palaeoecol.* 449, 41–51. doi:10.1016/j.palaeo.2016.02.005
- Ma, L., Wu, J., and Abuduwaili, J. (2016). Variation in Aeolian Environments Recorded by the Particle Size Distribution of Lacustrine Sediments in Ebinur Lake, Northwest China. *Springerplus* 5 (1), 481. doi:10.1186/s40064-016-2146-0
- Ma, Q., Zhu, L., Wang, J., Ju, J., Wang, Y., Lü, X., et al. (2020). Late Holocene Vegetation Responses to Climate Change and Human Impact on the central Tibetan Plateau. *Sci. Total Environ.* 708, 135370. doi:10.1016/j.scitotenv.2019.135370
- Maher, B. A., Prospero, J. M., Mackie, D., Gaiero, D., Hesse, P. P., and Balkanski, Y. (2010). Global Connections between Aeolian Dust, Climate and Ocean Biogeochemistry at the Present Day and at the Last Glacial Maximum. *Earth-Science Rev.* 99 (1-2), 61–97. doi:10.1016/j.earscirev.2009.12.001
- Morinaga, H., Itota, C., Isezaki, N., Goto, H., Yaskawa, K., Kusakabe, M., et al. (1993). Oxygen-18 and Carbon-13 Records for the Last 14,000 Years from Lacustrine Carbonates of Siling-Co (Lake) in the Qinghai-Tibetan Plateau. *Geophys. Res. Lett.* 20, 2909–2912. doi:10.1029/93GL02982
- Okin, G. S., Murray, B., and Schlesinger, W. H. (2001). Degradation of sandy Arid Shrubland Environments: Observations, Process Modelling, and Management Implications. *J. Arid Environments* 47 (2), 123–144. doi:10.1006/jare.2000.0711
- Pan, M., Wu, Y., Zheng, Y., and Tan, L. (2014). Holocene Aeolian Activity in the Dinggye Area (Southern Tibet, China). *Aeolian Res.* 12, 19–27. doi:10.1016/j.aeolia.2013.10.005
- Paterson, G. A., and Heslop, D. (2015). New Methods for Unmixing Sediment Grain Size Data. *Geochem. Geophys. Geosyst.* 16 (12), 4494–4506. doi:10.1002/2015gc006070
- Qiang, M., Chen, F., Zhang, J., Zu, R., Jin, M., Zhou, A., et al. (2007). Grain Size in Sediments from Lake Sugan: a Possible Linkage to Dust Storm Events at the Northern Margin of the Qinghai-Tibetan Plateau. *Environ. Geol.* 51 (7), 1229–1238. doi:10.1007/s00254-006-0416-9
- Qiang, M., Liu, Y., Jin, Y., Song, L., Huang, X., and Chen, F. (2014). Holocene Record of Eolian Activity from Genggahai Lake, Northeastern Qinghai-Tibetan Plateau, China. *Geophys. Res. Lett.* 41 (2), 589–595. doi:10.1002/2013gl058806
- Reimer, P. J., Bard, E., Bayliss, A., Beck, J. W., Blackwell, P. G., Ramsey, C. B., et al. (2013). Intcal13 and Marine13 Radiocarbon Age Calibration Curves 0–55,000 Years Cal Bp. *Radiocarbon* 55 (4), 1869–1887. doi:10.2458/azu_js_rc.55.16947
- Shi, X., Kirby, E., Furlong, K. P., Meng, K., Robinson, R., Lu, H., et al. (2017). Rapid and Punctuated Late Holocene Recession of Siling Co, central Tibet. *Quat. Sci. Rev.* 172, 15–31. doi:10.1016/j.quascirev.2017.07.017
- Sun, X. J., Du, N. Q., Chen, Y. S., Gu, Z. Y., Liu, J. Q., and Yuan, B. Y. (1993). Holocene Palynological Records in Lake Selincuo, Northern Xizang. *Acta Botanica Sinica* 35, 943–950.
- Sun, Z., Yuan, K., Hou, X., Ji, K., Li, C.-G., Wang, M., et al. (2020). Centennial-scale Interplay between the Indian Summer Monsoon and the Westerlies Revealed from Ngamring Co, Southern Tibetan Plateau. *The Holocene* 30 (8), 1163–1173. doi:10.1177/0959683620913930
- Thompson, L. G., Yao, T., Mosley-Thompson, E., Davis, M. E., Henderson, K. A., and Lin, P.-N. (2000). A High-Resolution Millennial Record of the South Asian Monsoon from Himalayan Ice Cores. *Science*, 289(5486), 1916–1919. doi:10.1126/science.289.5486.1916
- Wang, C., Wang, H., Song, G., and Zheng, M. (2019). Grain Size of Surface Sediments in Selin Co (central Tibet) Linked to Water Depth and Offshore Distance. *J. Paleolimnol.* 61 (2), 217–229. doi:10.1007/s10933-018-0054-8
- Wang, H., and Zheng, M. (2014). Lake Level Changes Indicated by Grain-Size of Core SL-1 Sediments since 5.33 Ka BP in Selin Co, Central Qinghai-Tibetan Plateau. *Sci. Tech. Rev.* 32 (35), 29–34. (in Chinese with English abstract). doi:10.3981/j.issn.1000-7857.2014.35.003
- Wang, K., Zhang, Y., Zhang, T., Yu, K., Guo, Y., and Ma, N. (2020). Analysis of Climate Change in the Selin Co Basin, Tibetan Plateau, from 1979 to 2017. *ARID ZONE RESEARCH* 37 (03), 652–662. (in Chinese with English abstract). doi:10.13866/j.azr.2020.03.13
- Wang, N., Yao, T., Pu, J., Zhang, Y., and Sun, W. (2006). Climatic and Environmental Changes over the Last Millennium Recorded in the Malan Ice Core from the Northern Tibetan Plateau. *Sci. China Ser. D* 49 (10), 1079–1089. doi:10.1007/s11430-006-1079-9
- Wang, Y., Cheng, H., Edwards, R. L., He, Y., Kong, X., An, Z., et al. (2005). The Holocene Asian Monsoon: Links to Solar Changes and North Atlantic Climate. *Science* 308 (5723), 854–857. doi:10.1126/science.1106296
- Wang, Y., Liu, X., Han, L., Ni, Z., Ma, X., Wei, Y., et al. (2021). Late Holocene Climate Variation on the Northern Tibetan Plateau Inferred from Lake Ayakum. *Catena* 207, 105599. doi:10.1016/j.catena.2021.105599
- Wang, Y., Wang, J., Zhu, L., Lin, X., Hu, J., Ma, Q., et al. (2017). Mid- to Late-Holocene Paleoenvironmental Changes Inferred from Organic Geochemical Proxies in Lake Tangra Yumco, Central Tibetan Plateau. *The Holocene* 27 (10), 1475–1486. doi:10.1177/0959683617693893
- Wang, Z., Zhang, H., Jing, X., and Wei, X. (2013). Effect of Non-spherical Dust Aerosol on its Direct Radiative Forcing. *Atmos. Res.* 120-121, 112–126. doi:10.1016/j.atmosres.2012.08.006
- Wolfe, S. A. (2022). “Cold-Climate Aeolian Environments,” in *Reference Module in Earth Systems and Environmental Sciences* (Elsevier), 195–219. doi:10.1016/B978-0-12-818234-5.00036-5
- Wu, G., Zhang, C., Xu, B., Mao, R., Joswiak, D., Wang, N., et al. (2013). Atmospheric Dust from a Shallow Ice Core from Tanggula: Implications for Drought in the central Tibetan Plateau over the Past 155 Years. *Quat. Sci. Rev.* 59, 57–66. doi:10.1016/j.quascirev.2012.10.003
- Wu, X., Li, X., Li, J., Wang, M., Ji, M., Cao, Y., et al. (2020). Eolian Dust Activity during the Last ~850 Years on the southeastern Margin of the Arid Central Asia. *Palaeogeogr. Palaeoclimatol. Palaeoecol.* 560, 110022. doi:10.1016/j.palaeo.2020.110022
- Xiao, J., Fan, J., Zhou, L., Zhai, D., Wen, R., and Qin, X. (2013). A Model for Linking Grain-Size Component to lake Level Status of a Modern Clastic lake. *J. Asian Earth Sci.* 69, 149–158. doi:10.1016/j.jseas.2012.07.003
- Xue, L., Zhang, Z. Q., Liu, W. M., Lv, T. Y., and Sun, J. M. (2010). The Shrinking Process of Siling Co in the Past 12 Ka: Based on OSL Dating of Past Shorelines. *Chin. J. Geology. (Scientia Geologica Sinica)* 45 (02), 428–439. (in Chinese with English abstract).
- Xuezi, M., Wang, Y. B., Yongbo, W., Chenchen, Z., and Zhenyu, N. (2019). Modern Sedimentary Process of Lake Basomtso in the southeastern Tibetan Plateau and its Response to Climate Change. *J. Lake Sci.* 31 (04), 1169–1181. (in Chinese with English abstract). doi:10.18307/2019.0403

- Yang, B., Bräuning, A., Zhang, Z., Dong, Z., and Esper, J. (2007). Dust Storm Frequency and its Relation to Climate Changes in Northern China during the Past 1000 Years. *Atmos. Environ.* 41 (40), 9288–9299. doi:10.1016/j.atmosenv.2007.09.025
- Yu, S., Wang, J., Li, Y., Peng, P., Kai, J., Kou, Q., et al. (2019). Spatial Distribution of Diatom Assemblages in the Surface Sediments of Selin Co, central Tibetan Plateau, China, and the Controlling Factors. *J. Great Lakes Res.* 45 (6), 1069–1079. doi:10.1016/j.jglr.2019.09.006
- Yu, X., Zhou, W., Franzen, L. G., Xian, F., Cheng, P., and Jull, A. J. T. (2006). High-resolution Peat Records for Holocene Monsoon History in the Eastern Tibetan Plateau. *Sci. China Ser. D* 49 (6), 615–621. doi:10.1007/s11430-006-0615-y
- Zhang, B., Liu, X., and Li, J. (2021). The Aeolian Component Inferred from lake Sediments in China. *Aeolian Res.* 50, 100700. doi:10.1016/j.aeolia.2021.100700
- Zhang, G., Yao, T., Xie, H., Zhang, K., and Zhu, F. (2014). Lakes' State and Abundance across the Tibetan Plateau. *Chin. Sci. Bull.* 59 (24), 3010–3021. doi:10.1007/s11434-014-0258-x
- Zhang, J., Ma, X., Qiang, M., Huang, X., Li, S., Guo, X., et al. (2016). Developing Inorganic Carbon-Based Radiocarbon Chronologies for Holocene lake Sediments in Arid NW China. *Quat. Sci. Rev.* 144, 66–82. doi:10.1016/j.quascirev.2016.05.034
- Zhang, P., Cheng, H., Edwards, R. L., Chen, F., Wang, Y., Yang, X., et al. (2008). A Test of Climate, Sun, and Culture Relationships from an 1810-year Chinese Cave Record. *Science* 322 (5903), 940–942. doi:10.1126/science.1163965
- Zhu, L., Lü, X., Wang, J., Peng, P., Kasper, T., Daut, G., et al. (2015). Climate Change on the Tibetan Plateau in Response to Shifting Atmospheric Circulation since the LGM. *Sci. Rep.* 5 (1), 13318. doi:10.1038/srep13318
- Conflict of Interest:** The authors declare that the research was conducted in the absence of any commercial or financial relationships that could be construed as a potential conflict of interest.
- Publisher's Note:** All claims expressed in this article are solely those of the authors and do not necessarily represent those of their affiliated organizations, or those of the publisher, the editors, and the reviewers. Any product that may be evaluated in this article, or claim that may be made by its manufacturer, is not guaranteed or endorsed by the publisher
- Copyright © 2022 Zhang, Zhang, Liu, Yao, Wan, Li, Hou and Zhang. This is an open-access article distributed under the terms of the Creative Commons Attribution License (CC BY). The use, distribution or reproduction in other forums is permitted, provided the original author(s) and the copyright owner(s) are credited and that the original publication in this journal is cited, in accordance with accepted academic practice. No use, distribution or reproduction is permitted which does not comply with these terms.